交通部中央氣象局

委託研究計畫期末成果報告

區域模式物理方法之改進及高解析度數值模式之降水預報研究

計畫類別：X 氣象　□海象

計畫編號：MOTC-CWB-99-2M-09

執行期間： 99 年 2 月 6 日至 99 年 12 月 31 日

計畫主持人： 陶爲國

執行機構： *Lanshing Hwang Landscape Architecture, Planning and Urban Design*

本成果報告包括以下應繳交之附件(或附錄)：See enclosed.

中華民國　99 年 12 月 2 日

政府研究計畫期末報告摘要資料表

計畫中文名稱	區域模式物理方法之改進及高解析度數值模式之降水預報研究		
計畫編號	MOTC-CWB-99-2M-09		
主管機關	交通部中央氣象局		
執行機構	*Lanshing Hwang Landscape Architecture, Planning and Urban Design*		
年度	99 年	執行期間	99 年 2 月 5 日至 99 年 12 月 31 日
本期經費 (單位：千元)	795　千元		
執行進度	預定（%）	實際（%）	比較（%）
	100	100	0
經費支用	預定(千元)	實際(千元)	支用率（%）
	795	795	100
研究人員	計畫主持人	協同主持人	研究助理
	陶爲國	張美玉	
報告頁數		使用語言	English
中英文關鍵詞	Weather, Numerical model, physical processes, heavy rainfall		
研究目的	(1) Continue improving, testing and evaluating the performance of the Goddard microphysical schemes and Goddard radiative processes in WRF. These two physical processes are being implemented into the WRF V 3.1.1 for CWB operational in Spring 2010, (2) Examine and modify the various microphysical processes (i.e., terminal velocity, condensation and evaporation rate) for 5-10 km grid spacing WRF simulations and, (3) Optimize/select a set of WRF's physical processes – a suite (a combination of particular microphysical, cumulus parameterization and planetary boundary layer schemes) for better QPF.		
研究成果	(1) Conduct the detailed case studies on the evaluating the performance of the improved microphysical and radiation scheme on surface rainfall forecast (2) Test the interactions between microphysics, PBL and cumulus parameterization for precipitation processes in WRF		

	(3) Identify the physical suite for WRF for improving the simulation of precipitation processes (especially for those of associated with impact weather events). 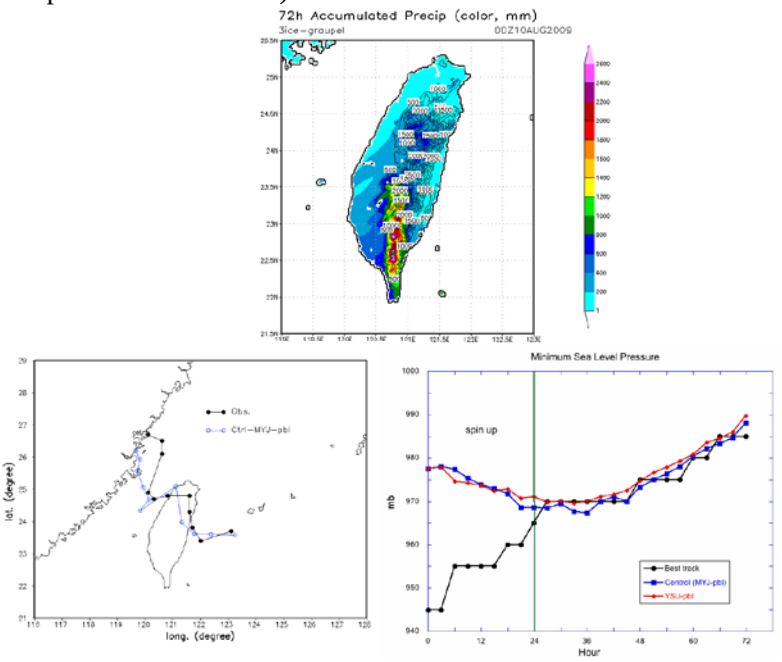 *Top: The model simulated accumulated rainfall from August 6 0000UTC to August 9 0000UTC 2009. The corresponding hurricane tracks (lower-left panel) and the Minimum sea level pressure (hPa) obtained from WRF forecasts (low-right panel) for Morakot case. The observed track and minimum sea level pressure (solid black line – from JMA) is also shown for comparison.*
具體落實應用情形	It is expected that these WRF modeling research at CWB can provide better precipitation and rainfall forecast and related information to the operational unit for reference and guidance
計畫變更說明	
落後原因	(若有)
檢討與建議(變更或落後之因應對策)	

中文摘要

近年來，台灣地區劇烈天氣系統(如颱風、局部豪大雨系統等)所帶來的強烈降水對於民生及經濟都有很大的損害。舉例來說，2009 年莫拉克颱風帶來的劇烈降水導致山崩，就造成了 600 多人的死亡。因此，改進高解析度模式之定量降水預報(Quantitative Precipitation Forecasts, QPF)便成為氣象局研究之首要需求之一。

本計畫將一個經過改進的雲物理及輻射參數化方法(包含其交互作用)放入目前最先進的數值模式 WRF(Weather and Research Forecast, WRF)之中，藉由模式中成雲過程的改進，使得颱風及其他劇烈天氣系統可以被較真實的模擬、預報及研究。

氣象局對此項研究委託計畫的主要目標，可總結為三個主要的部份：

(1) 持續改進、測試以及評估 WRF 模式中 Goddard microphysical schemes 以及 Goddard radiative processes 的效能。此二項物理過程已在 2010 年植入氣象局現行作業之 WRF V3.1.1 版本當中。

(2) 針對 WRF 模式 5-10 公里網格之模擬，檢查及修正其微物理過程(即終端速度、凝結與蒸發率)。

(3) 研究 WRF 模式中之物理過程－找出能產生較佳定量降水預報之組合(微物理、積雲參數化以及行星邊界層方法)。

可以預期這些 WRF 模式研究所產生之較佳的降水預報及其他相關資訊應可供作業單位做為有用的參考。

(1) 針對模式中改進之微物理及輻射方法對於地面降水預報的效能，做一詳盡的個案研究

(2) 測試在 WRF 模式中，微物理、輻射以及邊界層方法在降水過程中的交互作用

(3) 選取出 WRF 模式中對於降水過程有改善的最佳物理方法之組合(特別是對劇烈系統有改進者)

Summary

In recent years, the heavy rainfall that was associated with severe weather events (e.g., typhoons, local heavy precipitation events) has caused significant damages in the economy and loss of human life throughout Taiwan. For example, more than 600 people were dead due to the heavy rainfall – landslide associated with Typhoon Morakot 2009. An improvement of quantitative precipitation forecasts (QPF) using high-resolution numerical models should be one of the high priorities in CWB research.

An improved cloud microphysics and radiation (including their explicit interaction) parameterization has been implemented into the the-state-of-the-art Weather and Research Forecast (WRF) model. By adding the improved cloud processes in the WRF, the microphysics and their effect on precipitation processes, hurricane and other severe weather events can be realistic simulated, forecasted and studied.

The goals of this proposed CWB WRF modeling research are summarized into three major areas:

(4) Continue improving, testing and evaluating the performance of the Goddard microphysical schemes and Goddard radiative processes in WRF. These two physical processes are being implemented into WRF V 3.1.1 for CWB operational in 2010,
(5) Examine and modify the various microphysical processes (i.e., terminal velocity, condensation and evaporation rate) for 5-10 km grid spacing WRF simulations and,
(6) Investigate the WRF's physical process – suite (a combination of particular microphysical, cumulus parameterization and planetary boundary layer schemes) for better QPF.

It is expected that these WRF modeling research at CWB can provide better precipitation and rainfall forecast and related information to the operational unit for reference and guidance.

(4) Conduct the detailed case studies on the evaluating the performance of the improved microphysical and radiation scheme on surface rainfall forecast
(5) Test the interactions between microphysics, radiation and PBL for precipitation processes in WRF
(6) Identify the physical suite in WRF for improving the simulation of precipitation processes (especially for those of associated with impact weather events).

1. Introduction

In recent years, the heavy rainfall that was associated with severe weather events (e.g., typhoons, local heavy precipitation events) has caused significant damages in the economy and loss of human life throughout Taiwan. For example, Typhoon Morakot struck Taiwan on the night of Friday August 7th, 2009 as a category 2 storm with sustained winds of 85 knots (92 mph). Although the center made landfall in Hualien county along the central east coast of Taiwan and passed over the central northern part of the island, it was southern Taiwan that received the worst effects of the storm where locally as much as 2000 mm of rain were reported, resulting in the worst flooding there in 50 years. The result of the enormous amount of rain has been massive flooding and devastating mudslides. More than 600 people are confirmed dead (including hundreds of people in Shiao Lin, which was destroyed by a large mudslide). An improvement of quantitative precipitation forecasts (QPF) using numerical models should be one of the highest priorities in CWB research.

However, Taiwan's geographic feature causes a major challenge for predicting/forecasting heavy precipitation and its associated surface rainfall associated with Mei-Yu, MCS and typhoon. For example, two-thirds of Taiwan is mountainous, in particular, the Central Mountain Range (CRM) oriented in a north-south direction with averaged terrain height of 2000 m and a peak of 4000 m. With this unique orography, the mountains could not only generate its own local circulation, but also interact with large and mesoscale weather phenomena, such as Mei-Yu front, MCS and typhoon. In addition, Taiwan is a island with major moisture sources from south-western from South China Sea and dynamic and thermodynamic influences from a major continent (China).

Advances in computing power allow atmospheric prediction models to be run at progressively finer scales of resolution, using increasingly more sophisticated physical parameterizations and numerical methods. A report to the United States Weather Research Program (USWRP) Science Steering Committee calls for the replacement of implicit cumulus parameterization schemes with an explicit bulk microphysical scheme to improve QPF using the non-hydrostatic high-resolution numerical forecast model. The keys of the high resolution modeling system should also relay on the accuracy of the parameterization of complex physical processes (including their interactions), notably moist convective processes and land/ocean interaction with the atmosphere, and the understanding the resolution-dependence of the parameterized physical processes.

A sophisticated cloud microphysics and a radiative transfer parameterization (including their explicit cloud-radiation interaction) scheme have been recently implemented into a high-resolution non-hydrostatic weather research and forecast system (WRF). These two physical processes are being implemented into the WRF V 3.1.1 for operational in Spring 2010 a CWB. These two physical processes on precipitation and rainfall in the WRF still need to be investigated. Specifically, we will (1) test and improve the performance of the this cloud microphysical – radiative processes on severe weather events over Taiwan region, (2) examine the impact of different physical processes (i.e., interactions between cumulus parameterization and planetary boundary layer schemes) on QPF, and, (3) select a physical suite (a combination of particular microphysical, cumulus parameterization and planetary boundary layer schemes) for better QPF.
It is expected that these WRF modeling research at CWB can provide precipitation and rainfall forecast and related information to the operational unit for reference and guidance.

2. Methodology

(2.1) Weather Research and Forecast (WRF) Model

The WRF is a next-generation mesoscale forecast model and assimilation system that will be used to advance the understanding and the prediction of mesoscale precipitation systems. The model will incorporate advanced dynamics, numeric and data assimilation techniques, a multiple re-locatable nesting capability, and improved physical packages. The WRF model will be used for a wide range of applications, from idealized research to operational forecasting, with an emphasis on horizontal grid sizes in the range of 1-10 km. The WRF will be a candidate to replace existing research and forecast models (i.e., MM5, NCEP/ETA).

At Goddard, the modeling and dynamic group has implement several ice schemes (Tao *et al.* 2003a; Lang *et al.* 2007; Zeng *et al.* 2008 and Lang *et al.* 2010) into WRF V2.2.1, V3.1 and V3.2. The Goddard radiation (including explicitly calculated cloud optical properties) is recently implementing into and testing into WRF V3.1 and V3.2. WRF can also be initialized with the Goddard Earth Observing System (GEOS) global analyses. This link between the GEOS global analyses and the WRF models could allow for many useful regional modeling applications. For example, a series of weeklong WRF simulations were conducted to test the sensitivity of the initial and boundary conditions derived from NCEP, ECMWF, and GEOS on simulations of precipitation and chemistry (for air pollution study) transport over the eastern USA and East Asia.

(2.2) Microphysics scheme

The Goddard Cumulus Ensemble (GCE) model's (Tao and Simpson 1993) one-moment bulk microphysical schemes were implemented into WRF. These schemes are mainly based on Lin *et al.* (1983) with additional processes from Rutledge and Hobbs (1984). However, the Goddard microphysics schemes have several modifications. First, there is an option to choose either graupel or hail as the third class of ice (McCumber *et al.* 1991). Graupel has a relatively low density and a high intercept value (i.e., more numerous small particles). In contrast, hail has a relative high density and a low intercept value (i.e., more numerous large particles). These differences can affect not only the description of the hydrometeor population and formation of the anvil-stratiform region but also the relative importance of the microphysical-dynamical-radiative processes. Second, a new saturation technique (Tao *et al.* 1989) was added. This saturation technique is basically designed to ensure that super saturation (sub-saturation) cannot exist at a grid point that is clear (cloudy). The saturation scheme is one of the last microphysical processes to be computed. It is only done prior to evaluating evaporation of rain and deposition or sublimation of snow/graupel/hail. Third, all microphysical processes that do not involve melting, evaporation or sublimation (i.e., transfer rates from one type of hydrometeor to another) are calculated based on one thermodynamic state. This ensures that all of these processes are treated equally. The opposite approach is to have one particular process calculated first modifying the temperature and water vapor content (i.e., through latent heat release) before the next process is computed. Fourth, the sum of all sink processes associated with one species will not exceed its mass. This ensures that the water budget will be balanced in the microphysical calculations.

In addition to the two different 3ICE schemes (i.e., cloud ice, snow and graupel or cloud ice, snow and hail) implemented into WRF V2.2.1, V3.1 and V3.2, the Goddard microphysics has other two options. The first one is equivalent to a two-ice (2ICE) scheme having only cloud ice and snow. This option may be needed for coarse resolution simulations (i.e., > 5 km grid size). The two-class ice scheme could be applied for winter and frontal convection (Tao *et al.* 2009; Shi *et al.* 2010). The second one is a warm rain only (cloud water and rain). Recently, the Goddard 3ICE schemes were modified to reduce over-estimated and unrealistic amounts of cloud water and graupel in the stratiform region (Tao *et al.* 2003a; Lang *et al.* 2007). Various assumptions associated with the saturation technique were also revisited and examined (Tao *et al.* 2003a). A Spectral Bin Microphysical (SBM) scheme is recently implemented into WRF V3.1. The followings are recent modifications of Goddard scheme that was implemented into CWB WRF.

(a) An improved rain evaporation process

By comparing the bulk and spectral bin microphysics, it was found that the evaporation of rain in the bulk scheme is usually too large. An empirical correction factor—$r(qr) = 0.11q^{-1.27}r + 0.98$, where q_r is the rain mixing ratio (g kg^{-1})—is developed to correct the overestimation of rain evaporation in the bulk scheme (Li *et al.* 2009). Applying $r(q_r)$ in the bulk scheme produces spatial and temporal variation modes similar to those in sensitivity tests using the mean evaporation reduction factor. However, using $r(q_r)$ consistently results in a larger stratiform area. Similarly, it is possible to modify the ice phase microphysics in the bulk simulation using the bin scheme (see Fig. 1). However, ice phase microphysics has many uncertainties, including ice initiation and multiplication and the density, shape, and terminal fall velocity of various ice species and their interactions with one another. Many fundamental processes in ice microphysics are still being actively researched. Planned future study includes validating the ice microphysics in the bin scheme using both in situ and remote observations. After gaining confidence in the bin simulation, it will then be used to improve bulk microphysical schemes.

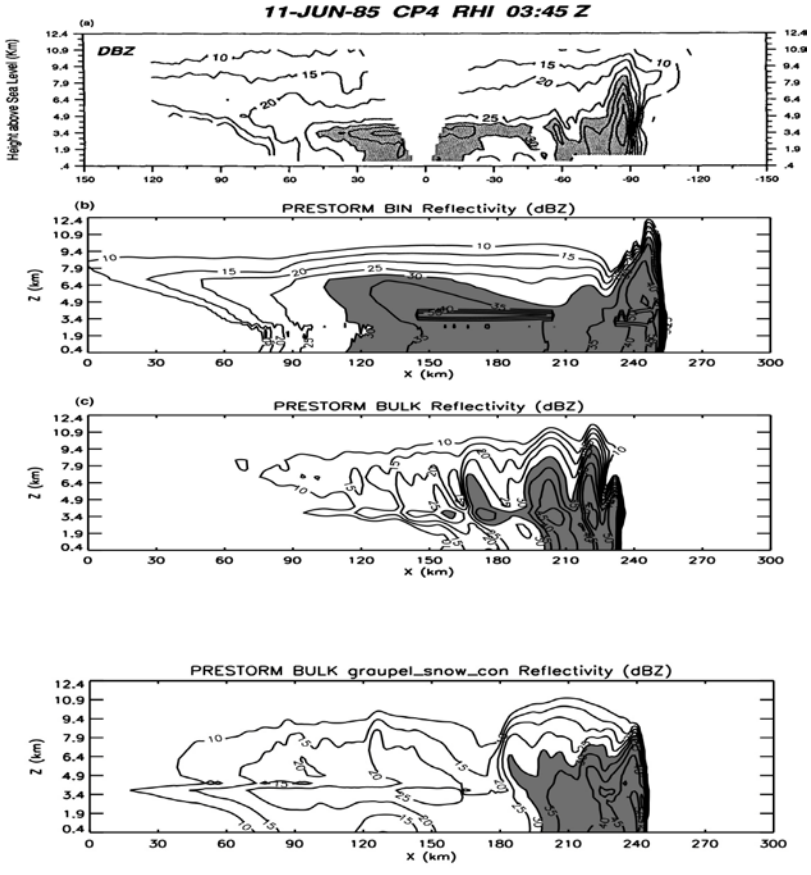

Fig. 1 Observed (top panel), GCE-spectral bin microphysics (beneath the top panel), GCE-bulk microphysics (above the bottom panel) and GCE-bulk-improved microphysics (bottom panel) simulated instantaneous radar reflectivity (dBZ).

Note that this modification is only valid for severe thunderstorms (i.e., cloud velocity is over 20 m/s) and for the Goddard 3-ICE scheme with hail option. This modification could be applied for summer thunderstorms occurred in Taiwan.

(b) An improved microphysical scheme to reduce 40dBz at high altitude

It is needed to continue examining and improving the performance of the WRF's bulk microphysics schemes. After the study by Lang *et al.* (2007), it was apparent that the bulk scheme required further modification, as there was still a noticeable bias in the simulated reflectivity distributions aloft with excessive probabilities at higher reflectivity values and peak values that were too strong. The bulk scheme was therefore systematically examined with each individual ice process re-evaluated in light of the aforementioned biases and the assumption that the overall scheme was producing either too much and/or graupel that was too large and possibly likewise for snow. Some logical improvements were made as well. As a result, the following changes to the scheme were adopted. First, in addition to not allowing dry growth[1] following Lang *et al.* (2007), graupel amounts were directly reduced by effectively lowering the overall riming efficiency, tightening the thresholds for converting rimed snow to graupel, and allowing graupel to sublimate outside of cloud, which was not allowed in the original formulation. As cloud is assumed mono-disperse (i.e., having a constant diameter of 20 microns), the graupel riming efficiency was made a function just of graupel size with smaller sizes less efficient and larger sizes more efficient (e.g., Khain *et al.* 2001). The riming thresholds for converting snow into graupel are fairly arbitrary but can have a large impact on graupel production (Rutledge and Hobbs 1984; Morrison *et al.* 2008); however, based on comparisons with satellite and radar data (e.g., Lang *et al.* 2007), the scheme is almost certainly producing too much graupel. The thresholds were therefore adjusted to reduce the amount of graupel, which resulted in more snow. Graupel amounts were also reduced indirectly by reducing the amount of super-cooled cloud water available for riming. The original scheme lacked sufficient means to realistically convert cloud water to cloud ice in the mixed-phase region and relied on somewhat ad hoc settings in the saturation adjust scheme to compensate. Outside of riming, the original scheme did not have the means to convert appreciable amounts of cloud liquid water into ice by the time air parcel temperatures fell to between -12 and -18^{o} C where very little liquid water is typically observed (e.g., Stith *et al.* 2002). To remedy this, three new processes were added: rime splintering, immersion freezing and contact nucleation. In addition, the original Fletcher (1962) curve for the number of activated ice nuclei was replaced with the Meyers *et al.* (1992) formulation throughout the code. In conjunction with these changes, the sequential saturation scheme was relaxed. Water saturation, which is calculated first, was allowed to occur down to much colder temperatures followed by ice saturation, which was allowed to be super saturated as is commonly observed (Jensen *et al.* 2001; Stith *et al.* 2002). Preliminary testing showed that these changes alone were not enough to effectively reduce excessive simulated reflectivities at upper levels, so in addition to reducing the amount of graupel, a size-mapping scheme was introduced whereby the characteristic size (i.e., inverse of the slope parameter) of the inverse

[1] Dry growth may not be absolutely zero but should be quite small. Efficiencies are commonly set to very small values.

exponential graupel distribution was specified based on temperature and graupel mixing ratio, effectively lowering the size of graupel particles at colder temperatures while still allowing particles to be large near the melting level and at higher mixing ratios[2]. In addition to these changes to graupel, similar changes were required for snow to bring the core reflectivity probabilities more in line with observations. Snow amounts were reduced by effectively lowering the overall collection efficiency of cloud ice by snow (by again making the efficiency dependent on collector particle size with smaller sizes having a very low efficiency and larger sizes a moderate efficiency), allowing snow to sublimate outside of cloud (not allowed in the original formulation) and accounting for the ambient relative humidity and size of the cloud ice particles in the "Bergeron" process (i.e., Psfi) where cloud ice crystals grow into snow. In the original formulation for Psfi, the ambient relative humidity is implicitly assumed to be 100% with respect to water, which is often incorrect. As will graupel, the characteristic sizes for snow were also mapped according to temperature and mixing ratio with small sizes at colder temperatures and low mixing ratios and larger sizes near the melting level and at higher mixing ratios. In addition to these changes, cloud ice fall speeds were added and accounted for in the sweep volume of those processes involving the accretion of cloud ice. Finally, the threshold for cloud ice auto-conversion to snow was changed to physical units. Table 1 gives a summary of all of the changes along with more details. Figure 2 shows time-height cross sections of maximum reflectivity simulated from the model using the new microphysics modifications, the original scheme and observations.

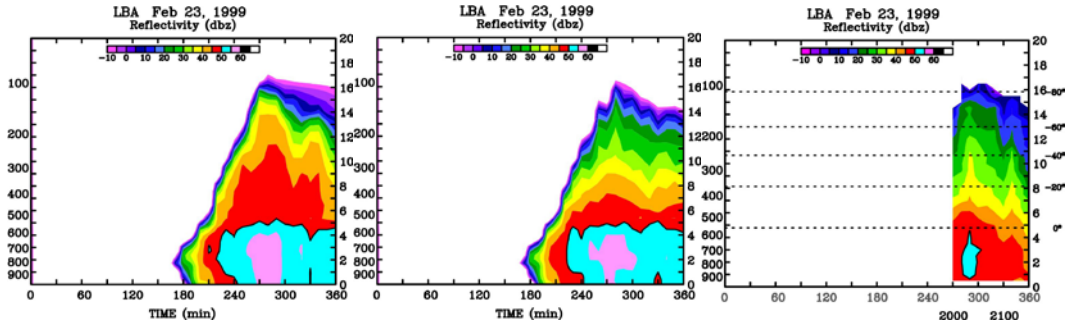

Fig. 2 Time-height cross sections of maximum radar reflectivity obtained from 3D simulations of the 23 February 1999 easterly regime event observed during TRMM LBA (Large Scale Biosphere-Atmosphere Experiment in Amazonia) using the original Rutledge and Hobbs (1984) based bulk microphysics formulation (left panel), an improved version (midde panel) and observed (right panel). Climatologically, 40-dBZ penetrations above 10 km are rare even over land (Zipser et al. 2006; Liu et al. 2008). Ground-based radar data for this case indicated 40-dBZ echoes reached to approximately 8 km.

[2] Previous studies have varied the snow/graupel intercept as a function of either mixing ratio (Swann 1998; Reisner *et al.* 1998; Thompson *et al.* 2004) or temperature (Thompson *et al.* 2004; Hong *et al.* 2004).

Process	Original	Modified	Reference(s)/Notes
Psaut	Efficiency: f(Tair)	Efficiency fixed, threshold: changed from g/g to g/m^{-3}	
Psaci	Esi = 0.1	Esi is f(snow diameter)	See mapping, Fig. X for size distribution for size distribution
Praci		Accounts for addition of cloud ice fall speed	Cloud ice fall speed follows Hong et al. (2004)
Psfi	Independent of RH	Depends on RH, accounts for cloud ice size via Meyers, which depends on ssi	Meyers et al. (1992)
Dgacs/Dgaci		Turned off	See Lang et al. (2007)
Dgacw	Egc = 1.0	Egc is f(graupel diameter)	See mapping, Fig. X for size distribution
Psacw/Pwacs	Esc = 1.0, Qc0 = 0.5 g/kg	Esc = 0.45, Qc0 = 1.0 g/kg	
Rime splintering	None	Added and applied to Psacw/Pgacw, no f(Vs/g) or f(cloud size)	Hallet and Mossop (1974); f(Tair) and splinter mass follow Ferrier (1994)
Pidw/Pidep	Based on Fletcher	Based on Meyers, which depends on ssi	Fletcher (1962); Meyers et al. (1992)
Pint	Based on Fletcher	Based on Meyers, which depends on ssi, previous ice concentration checked	Fletcher (1962); Meyers et al. (1992)
Immersion Freezing	None	Added based on Diehl	Diehl and Wurzler (2004); Diehl et al. (2006), assumes Bh,i = 1.01 e-2 for pollen
Contact Nucleation	None	Added based on Cotton and Pruppacher for Brownian diffusion only	Cotton et al. (1986); Pruppacher and Klett (1980), 500 active nuclei per cc with radii of 0.1 microns
Saturation Adjustment	Sequential based Tao	Modified sequential, iterative, allows for ssi of up to 10%	Tao et al. (2003)
Snow/Graupel Sublimation	None	Allowed if outside cloud and air subsaturated	
Snow/Graupel size	Based on fixed intercepts	Based on intercepts mapped according to snow/graupel mass and temperature	
Cloud ice fall Speed	None or based on Starr and Cox	Based on Hong	Hong et al. (2004); Starr and Cox (1985)

Table 1. Microphysical processes modified or added to the original GCE Rutledge and Hobbs based bulk microphysics scheme. "f( )" indicates "function of". Esi, Egc, and Esc are the collection efficiencies of cloud ice by snow, cloud by graupel and cloud by snow, respectively. Qc0 is the cloud water mixing ratio and ssi, the supersaturation percentage with respect to ice, RH the relative humidity, Vs/g the snow/graupel fall velocity, Bh,i the immersion mode ice nucleating efficiency, and Tair the air temperature. The process nomenclature essentially follows Lin et al. (1983) and Rutledge and Hobbs (1983,1984). Dgacs and Dgaci are the graupel collection of snow and cloud ice for the dry mode, respectively, and Dgacw the graupel collection of cloud at temperature below freezing.

(2.3) Radiation

(a) Radiative Transfer

The parameterizations developed by Chou and Suarez (1999) for shortwave radiation and by Chou *et al.* (1995), Chou and Kouvaris (1991), Chou *et al.* (1999), and Kratz *et al.* (1998) for longwave radiation have been implemented into the WRF model. The solar radiation scheme

includes absorption due to water vapor, CO_2, O_3, and O_2. Interactions among the gaseous absorption and scattering by clouds, aerosols, molecules (Rayleigh scattering), and the surface are fully taken into account. Fluxes are integrated virtually over the entire spectrum, from 0.175 μm to 10 μm. The spectrum is divided into seven bands in the ultraviolet (UV) region (0.175-0.4 μm), one band in the photosynthetically active radiation (PAR) region (0.4-0.7 μm), and three bands in the near infrared region (0.7-0.10 μm). In the UV and PAR region, a single O_3 absorption coefficient and a Rayleigh scattering coefficient are used for each of the eight bands. The O_3 absorption coefficient is taken from the spectral values given in WMO (1985). In the infrared, the k-distribution method is applied to compute the absorption of solar radiation. Ten k-distribution functions (equivalently, ten k values) are used in each of the three bands. The one-parameter scaling is used to compute the absorption coefficient in individual layers where temperature and pressure vary with height. The absorption due to O_2 is derived from a simple function, and the absorption due to CO_2 is derived from pre-computed tables. Reflection and transmission of a cloud and aerosol-laden layer are computed using the d-Eddington approximation. Fluxes for a composite of layers are then computed using the two-stream adding approximation.

In computing thermal infrared fluxes, the spectrum is divided into nine bands. As in the solar spectral region, the k-distribution method with temperature and pressure scaling is used to compute the transmission function in the weak absorption bands of water vapor and minor trace gases (N_2O, CH_4, CFC's). Six values of k are used for water vapor absorption, and only a few values of k are used for the minor trace gases. For the strong absorption bands of water vapor, the 15-μm CO_2 band, and the 9.6-μm O_3 band, the cooling is strong in the upper stratosphere. The use of the k-distribution method with the one-parameter temperature and pressure scaling induces a large error in the cooling rate above the 10-mb level. Instead, a look-up table method is used to compute the transmission function in the strong absorption bands, which computes accurately the cooling rate from the surface to the 0.01-mb level.

(b) Cloud Optical Properties

The use of a fully explicit microphysics scheme (liquid and ice) and a fine horizontal resolution (5 km or less) can simulate realistic cloud optical properties, which are crucial for determining the radiation budgets. With high spatial resolution, each atmospheric layer is considered either completely cloudy (overcast) or clear. No partial cloudiness is assumed. For detailed discussion on cloud optical properties can be found in Tao *et a*l. (2003).

Predicted radiative cooling and heating rates at cloud-top from both methods are on the order of 30 to 50 ^{o}K/day, which is in good agreement with Ackerman *et al*. (1988) and Stephens (1978). Sensitivity tests have been performed to examine the impact of various cloud optical property calculations on rainfall. The results show that the impact of the various cloud optical property calculations is greater in tropical cases, 3-5% compared to just 1-2% for mid-latitude cases.

(2.4) The planetary boundary layer (PBL)

The planetary boundary layer (PBL) is basically responsible for vertical sub-grid-scale fluxes due to eddy transports in the whole atmospheric column, not just the boundary layer. Thus, when a PBL scheme is activated, explicit vertical diffusion is de-activated with the assumption that the

PBL scheme will handle this process. The PBL schemes determine the flux profiles within the well-mixed boundary layer and the stable layer, and thus provide atmospheric tendencies of temperature, moisture (including clouds), and horizontal momentum in the entire atmospheric column. Most PBL schemes consider dry mixing, but can also include saturation effects in the vertical stability that determines the mixing. The schemes are one-dimensional, and assume that there is a clear scale separation between sub-grid eddies and resolved eddies. This assumption will become less clear at grid sizes below a few hundred meters, where boundary layer eddies may start to be resolved, and in these situations the scheme should be replaced by a fully three-dimensional local sub-grid turbulence scheme such as the Turbulence Kinetic Energy (TKE) diffusion scheme. It is important to understand how assumptions regarding the character of surface fluxes and vertical mixing within the boundary layer impact simulations of convective systems (and typhoons). Two different PBL schemes

(a) Yonsei University (YSU) PBL

The YSU PBL scheme (Hong *et al.* 2006) is the new version of the Medium-Range Forecast (MRF) PBL scheme (Hong and Pan 1996). This PBL scheme employs a so-called counter-gradient flux for heat and moisture in unstable conditions. It uses enhanced vertical flux coefficients in the PBL, and the PBL height is determined from a critical bulk Richardson number. It handles vertical diffusion with an implicit local scheme, and it is based on local Ri in the free atmosphere. The major strength of the YSU scheme is the inclusion of an explicit treatment of entrainment processes at the top of the PBL and the use of the counter-gradient terms to represent fluxes due to non-local gradients. The entrainment is made proportional to the surface buoyancy flux in line with results from studies with large-eddy models. The YSU scheme improves the MRF scheme by including an explicit treatment of entrainment process at the top of the PBL, which can help to avoid the excessive mixing in the mixed layer during strong wind events. The PBL top is defined using a critical bulk Richardson number of zero (compared to 0.5 in the MRF PBL), so is effectively only dependent on the buoyancy profile which, in general, lowers the calculated PBL top compared to MRF.

In YSU scheme, the PBL height is defined as a level where minimum flux exists inside the inversion layer; according to Hong *et al.* (2006), in the mixed layer-region (z<=h) the turbulence diffusion equation for a generic prognostic variable, C is:

$$\frac{\partial C}{\partial t} = \frac{\partial}{\partial z}\left[K_c\left(\frac{\partial C}{\partial z} - \gamma_c\right) - \overline{(w'c')_h}\left(\frac{z}{h}\right)^3 \right] \qquad (1)$$

Where K_c is the turbulent diffusion coefficient, γ_c is a correction factor to the local gradient which incorporates the contribution of the large-scale eddies to the total flux, and the second term on the right-hand side represents the asymptotic entrainment flux in the inversion layer. The term $\overline{(w'c')_h}$ is the flux at the inversion layer, w' is the vertical velocity perturbation and c' is the perturbation term for C. The formula keeps the basic concept of Hong et al. (1996) but includes an asymptotic entrainment flux term at the inversion layer $-\overline{(w'c')_h}\left(\frac{z}{h}\right)^3$, which is not included (1996). Thus, the major difference from Hong *et al.* (1996) is the *explicit treatment* of the entrainment processes through the second term on the rhs of (1), whereas the entrainment is *implicitly parameterized* by raising *h* above the minimum flux level in Hong *et al.* (1996). Above

the mixed layer ($z > h$), a local diffusion approach is applied to account for free atmospheric diffusion. In the free atmosphere, the turbulent mixing length and stability formula based on observations (Kim and Mahrt (1992) are utilized. The penetration of entrainment flux above h in Noh *et al.* (2003) is also considered. Please refer to Hong *et al.* (2006) for a more comprehensive description of the YSU scheme.

(b) Mellor-Yamada-Janjic (MYJ) PBL

This parameterization of turbulence in the PBL and in the free atmosphere (Janjic, 1990, 1996, 2002) represents a nonsingular implementation of the Mellor-Yamada Level 2.5 turbulence closure model (Mellor and Yamada, 1982) through the full range of atmospheric turbulent regimes. In this implementation, an upper limit is imposed on the master length scale. This upper limit depends on the TKE as well as the buoyancy and shear of the driving flow. In the unstable range, the functional form of the upper limit is derived from the requirement that the TKE production be nonsingular in the case of growing turbulence. In the stable range, the upper limit is derived from the requirement that the ratio of the variance of the vertical velocity deviation and TKE cannot be smaller than that corresponding to the regime of vanishing turbulence. The TKE production/dissipation differential equation is solved iteratively. The empirical constants have been revised as well (Janjic, 1996, 2002).

The YSU and MYJ PBL schemes differ in their ways of calculating the surface fluxes and the vertical mixing in the PBL. The YSU PBL scheme is a "non-local *K*" scheme. This approach uses the counter-gradient fluxes to determine the depth of the PBL, and then constrains the vertical diffusion coefficient to a fixed profile within the PBL. The MYJ scheme, however, is a "local *K*" scheme. The diffusivity coefficients are parameterized as functions of the local Richardson number. The height of the MYJ PBL is estimated from the TKE production. The non-singularity constraint for the TKE production is used under unstable atmosphere conditions.

Note that both YSU and MYJ PBL scheme need to be used in combination with a Smagorinsky first-order closure approach (Smagorinsky, 1963) which independently handles the horizontal turbulent mixing as a function of the horizontal deformation tensor.

(2.4) Cumulus Parameterization

The primary task of cumulus parameterization is to estimate the rate of sub-grid scale convective precipitation and its associated latent heat release, as well as the redistribution of moisture and momentum in the vertical. These quantities must be linked to the resolvable scale, which strongly depends on the horizontal resolution used in the model (Frank, 1983; Molinari and Dudek, 1992). Generally speaking, almost all cumulus parameterization schemes have three major components: (1) a trigger function to activate the parameterization; (2) a cloud model to estimate the convective properties as a function of the grid-scale variables; and (3) a closure to determine the total amount of convection. For example, Xu and Arakawa (1992) used the following equation to evaluate the Arakawa and Schubert (1974) cumulus parameterization:

$$\frac{DA}{Dt} = -kM_B + F \qquad (2)$$

where the variable F is the large-scale forcing or trigger function (*e.g.*, low-level instability, mass convergence and/or moisture convergence); $-kM_B$ is an adjustment by the clouds (usually determined by a cloud model), and A is the cloud working function. In order to close the whole cumulus parameterization, Arakawa and Schubert (1974) assumed that DA/Dt = 0 (called quasi-equilibrium). In order to understand the performance of a cumulus parameterization scheme, it is necessary to examine how these three components function individually as well as how they interact with each other within the various schemes.

Several cumulus parameterization schemes have been implemented into the WRF. The following is a brief review of three cumulus parameterization schemes that have bee used the most.

(a) Kain-Fritsch (KF-Eta)

Fritsch and Chappell (1980) scheme depends on the instantaneous stability of the environment. After adjustment, this scheme will produce an equilibrium state in terms of static stability. This scheme is related to resolved destabilizing processes through a convective trigger function. Kain and Fritsch (1990, 1993) have developed a sorting technique that simulates entrainment and detrainment processes using a spectrum of mixing events. This scheme allows the vertical distribution of convective heating and moistening tendencies to vary realistically as a function of the thermodynamic environment of parameterized clouds. This scheme has been modified based on testing within Eta model. It differs from the original KF scheme as the followings:

Shallow convection (non-precipitation) convection is allowed for any updraft that does not reach minimum cloud depth for precipitating clouds (this minimum depth varies as a function of cloud based temperature).

The entrainment rate is allowed to vary as a function of low-level convergence. Also the minimum entrainment rate is imposed to suppress widespread convection in marginally unstable, relative dry environment.

The properties of the downdraft is also changed in terms of source layer (entire 150-200 mb deep just above cloud base), detrainment (specified to occur in updraft source layer and above), and mass flux (specified as a function of updraft mass flux at cloud base, and as a function of source layer relative humidity rather than the wind shear or precipitation efficiency).

(b) Betts-Miller-Janjic (BMJ)

Betts and Miller (Betts, 1986; Betts and Miller, 1986) have developed a sophisticated convective adjustment scheme (adjusts the lapse rate to neutrality within a specified time interval). In their scheme, temperature and moisture profiles are relaxed toward reference profiles derived from quasi-equilibrium assumptions over some time period. This time period is used to determine the lag between convection and large-scale trigger (forcing). The shallow and deep convective reference profiles are different (one by forcing the sum of the condensation and precipitation to be zero and the other by a total enthalpy constraint). The Betts-Miller-Janjic (BJM, Janjic, 1994, 2000) scheme differs from the Betts and Miller in the followings: (1) the deep convection profiles and the relaxation time are variable and depend on the cloud efficiency (a non-dimensional parameter that characterizes the convective regime). (2)

The cloud efficiency depends on the entropy change, precipitation, and mean temperature of the cloud. (3) The shallow convection moisture profile is derived from the requirement that the entropy change be small and nonnegative.

Recently, BMJ scheme has been optimized for higher horizontal resolutions, primarily through modifications of the triggering mechanism (i.e., for the entropy change in the cloud is set up below which the deep convection is not triggered; the ascending particle mixes with the environment in searching for the cloud top; and the work of the buoyancy force on the ascending particle is required to exceed a prescribed positive threshold).

(c) Grell and Devenyi Ensemble Scheme

Grell and Devenyi (2002) introduced an ensemble cumulus scheme in which effectively multiple cumulus schemes and variants are run within each grid box and then the results are averaged to give the feedback to the model. In principle, the averaging can be weighted to optimize the scheme, but the default is an equal weight. The schemes are all mass-flux type schemes, but with differing updraft and downdraft entrainment and detrainment parameters, and precipitation efficiencies. These differences in static control are combined with differences in dynamic control, which is the method of determining cloud mass flux. The dynamic control closures are based on convective available potential energy (CAPE or cloud work function), low-level vertical velocity, or moisture convergence. Those based on CAPE either balance the rate of change of CAPE or relax the CAPE to a climatologically value, or remove the CAPE in a convective time scale. The moisture convergence closure balances the cloud rainfall to the integrated vertical advection of moisture. Another control is the trigger, where the maximum cap strength that permits convection can be varied. These controls typically provide ensembles of 144 members.

3. Results

3.1 Conduct high-resolution model simulations for Typhoon Morakot (2009)

Typhoon Morakot struck Taiwan on the night of Friday August 7th, 2009 as a category 2 storm with sustained winds of 85 knots (92 mph). Although the center made landfall in Hualien county along the central east coast of Taiwan and passed over the central northern part of the island, it was southern Taiwan that received the worst effects of the storm where locally as much as 3000 mm of rain were reported, resulting in the worst flooding there in 50 years. Nearly the entire southern half of the island has in excess of 600 mm (~24 inches, shown in yellow shading) of rain. Within that are two areas in excess of 1000 mm (~40 inches, shown in red) along the western slopes of the central mountain range. The result of the enormous amount of rain has been massive flooding and devastating mudslides. More than 700 people lost their life including hundreds of people in Shiao Lin, which was destroyed by a large mudslide. Shiao Lin is located on the western side of the central mountain range in south central Taiwan.

We have conducted sensitivity tests in terms of model grid mesh for a heavy precipitation event. The WRF V3.1 with improved microphysics is used to simulate this typhoon case. Fig. 3 shows the WRF domain, with 18, 6 and 2 km with corresponding numbers of grid points 391x322x61, 475x427x61, 538x439x61, respectively. Time steps of 18, 6 and 2 seconds are used in these

nested grids, respectively. The Grell-Devenyi (2002) cumulus parameterization scheme was used for the outer grid (18 km) only. For the inner two domains (6 and 2 km), the Grell-Devenyi parameterization scheme was turned off. The planetary boundary layer parameterization employed the Mellor-Yamada-Janjic (Mellor and Yamada 1992) turbulence closure model. The surface heat and moisture fluxes (from both ocean and land) were computed from similarity theory (Monin and Obukhov 1954). The land surface model is based on Chen and Dudhia (2001). It is a 4-layer soil temperature and moisture model with canopy moisture and snow cover prediction. The Goddard broadband two-stream (upward and downward fluxes) approach was used for the shortwave and longwave radiative flux calculations (Chou and Suarez 1999). The model was initialized from NOAA/NCEP/GFS global analyses (1.0^{o} by 1.0^{o}). Time-varying lateral boundary conditions were provided at 6-h intervals.

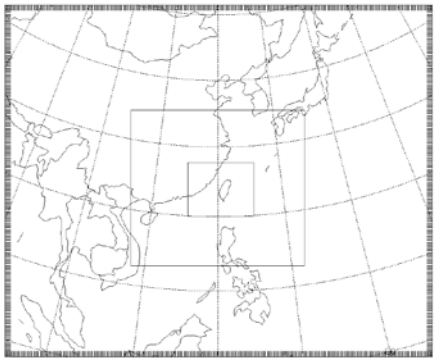

Fig. 3 WRF Inter-nesting model configuration used for Typhoon Moratok case. Horizontal resolutions for domains are 18, 6 and 2 km, respectively.

Figure 4 shows the simulated MSLP and track from WRF using 2 km grid domain. The simulated hurricane is in very good agreement with observation after 24 h model integration. However, the first 24 h is weaker than observation due to the fact that no initial bogus is used (model requires spin up). The simulated tracks are generally also captured observed. However, the track error becomes larger in the high terrain area and in the middle Taiwan Strait (the typhoon moves out of the 2 km grid domain).

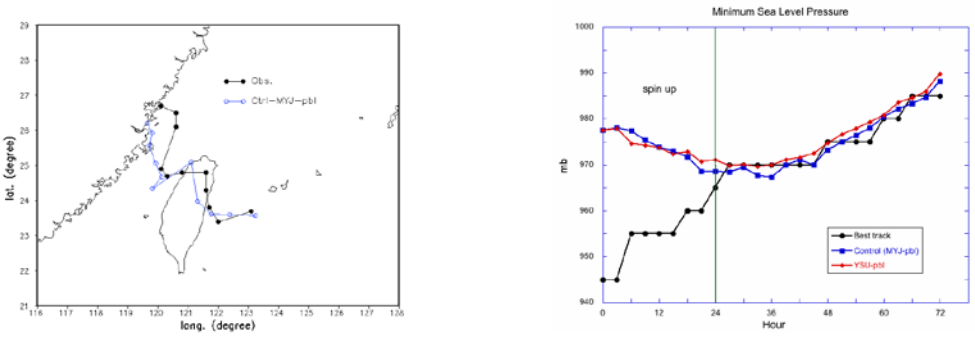

Fig. 4 The corresponding hurricane tracks (left panel) and the Minimum sea level pressure (hPa) obtained from WRF forecasts (right panel) for Morakot case. The observed track and minimum sea level pressure (solid black line – from JMA) is also shown for comparison.

Figure 5 shows the observed and WRF-simulated rainfall using three different options (improved and original 3ICE-graupel) and warm rain only in the Goddard microphysical

scheme. Generally speaking, WRF produced the right distribution of precipitation for this typhoon case despite using different Goddard microphysical options. For example, in all of the runs the main precipitation event is elongated in the southwest-northeast direction and concentrated in a heavy north-south line over southern Taiwan as observed. All options resulted in simulations wherein the main area of precipitation continued over southern Taiwan over the 72-h period. This feature also generally agrees with observations. The results (with high resolution visualization) show that a persistent (over 48 h) southwesterly flow associated with Morakot and its circulation was able to draw up copious amounts of moisture from the South China Sea into southern Taiwan where it was able to interact with the steep topography in all four microphysical options. These results suggest that the main rainfall distribution in the Morakot case is determined by the large-scale circulation pattern (i.e., the typhoon-induced circulation). The interaction between the terrain and moisture flux was the dominant factor that led to the floods/landslides in this case. All of the options produced more than 2000 mm of accumulated rainfall over southern Taiwan. Also, the improved 3ICE-graupel produced more rainfall over northeastern Taiwan, which may be in better agreement with observations than other schemes (see Fig. 5). In addition, the warm rain only almost similar results as other two cases in terms of rainfall pattern, maximum rainfall and total amount rain over South Taiwan and whole Island (Fig. 6). These results suggested that the warm rain processes are dominant for precipitation processes.

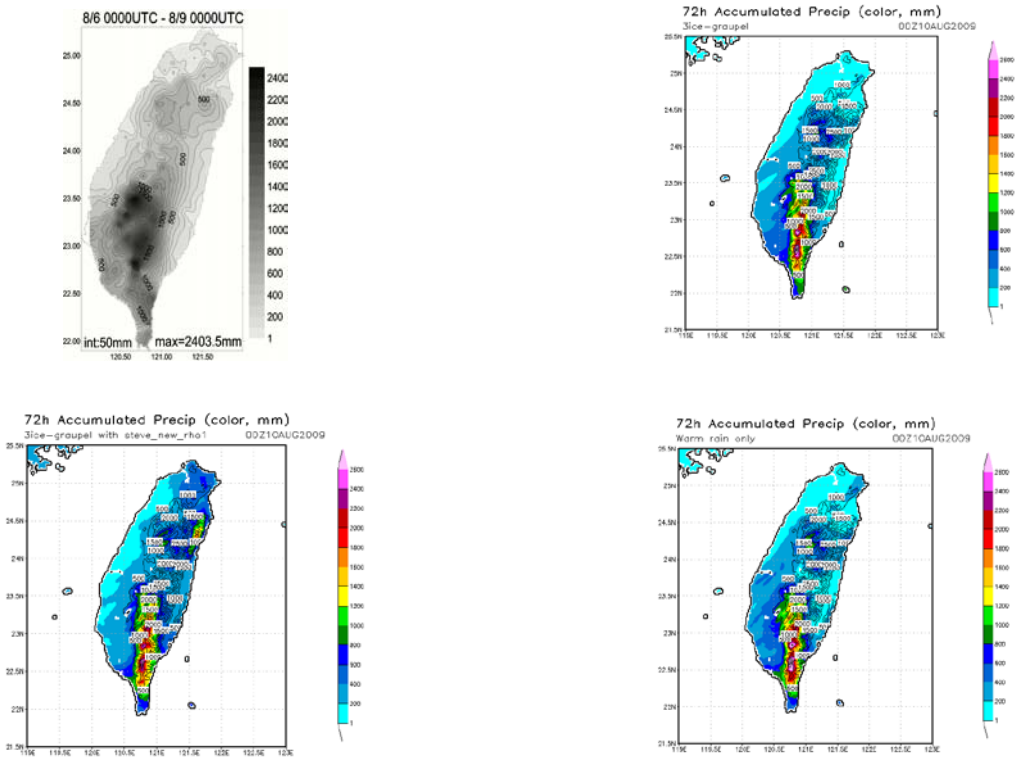

Fig. 5 Observed (left-top) and model simulated accumulated rainfall from August 6 0000UTC to August 9 0000UTC 2009. The original (right-top), improved (left-bottom) and warm rain only (right-bottom) are shown for comparison with observation.

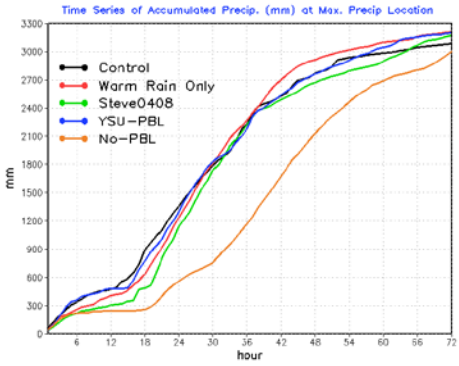

Fig. 6 *Time series of model simulated accumulated rainfall for control, warm rain only, improved microphysics, YSU-PBL and No-PBL case.*

Figure 7 shows the time series of rainfall at three different latitude lines, 23.5^0N, 23.0^0N, and 22.5^0N, respectively. The results indicated that the rain cells mainly propagate from ocean into coast and high terrain region at high latitudes (23.5^0N, 23.0^0N). On the other hand, the rain cells propagate from southwest into coast and terrain region. There are two major sources of moisture and precipitation for the heavy rainfall over south Taiwan. The typhoon-induced circulation causes the first one. Then the southwestern moisture from South China Sea provided another heavy rainfall. With high-resolution (temporal and spatial) visualization of tracer transport and rain movements[3], the origins of these rain cells are clearly shown.

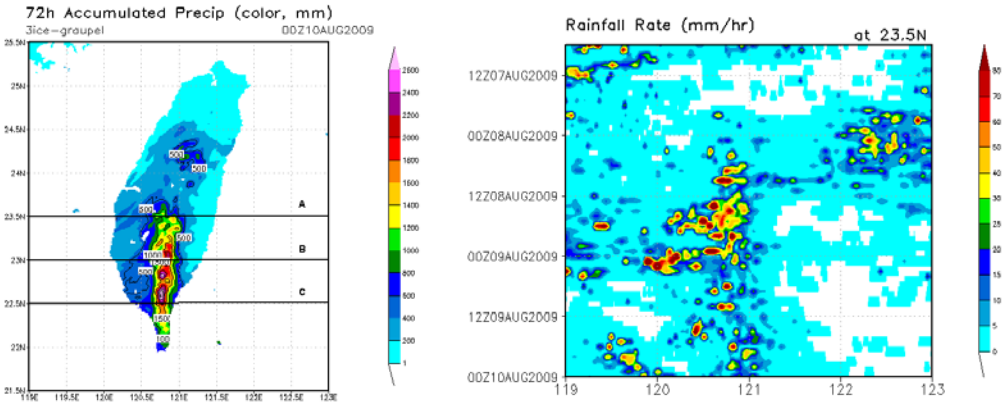

[3] PI has provided these high-resolution visualizations to Co-I and CWB during his February visit.

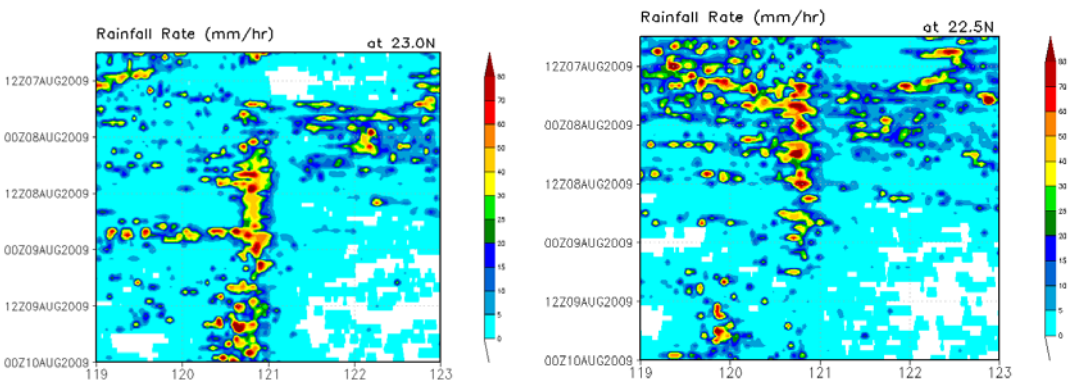

Fig. 7 Time series (Hovmollar diagrams) of rainfall at three different latitude lines (23.5^0N, 23.0^0N, and 22.5^0N).

Figure 8 shows the model simulated accumulated rainfall and averaged rain rates at different terrain regions, less than 100 m, between 100-500m, 500-1500 m, 1500-2500 m and higher than 2500 m. The results indicated that the most surface rainfall occurred at area over 1500 m and above. The model results also indicated that the rain intensity is quite small for low terrain region compared to those high terrain regions (Table 2). One interesting result is that the maximum rainfall intensity is weaker for area over 2500 m than those are between 500 – 2500 m. This is because that the 2500 m is near at top of terrain and the terrain-induced rain might be less significant than those areas lower. This suggested that the terrain-induced circulation (i.e., upward motion) could enhance precipitation processes and increase the rainfall intensity.

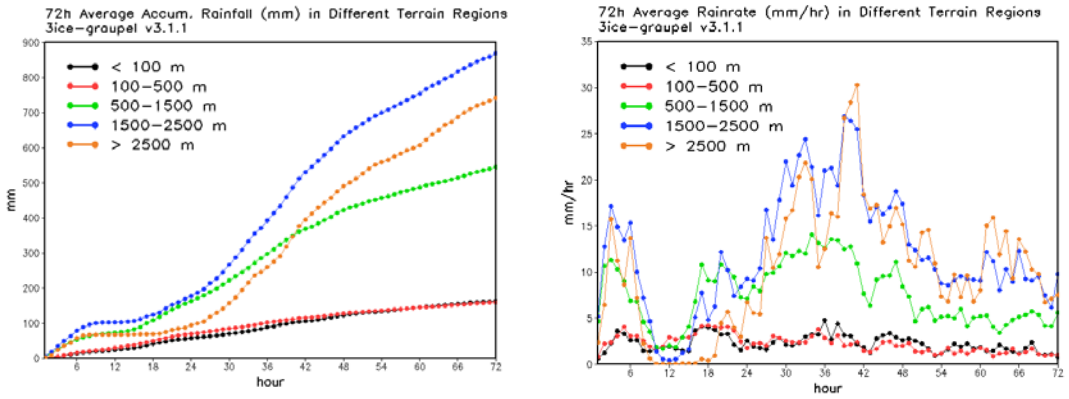

Fig. 8 Model simulated accumulated rainfall (left panel) and averaged rain rates (right panel) at different terrain regions from August 6 0000UTC to August 9 0000UTC 2009.

Altitude	Maximum Accumulated rainfall (mm)	Maximum rainfall intensity (mm/h)	Averaged Accumulated rainfall (mm)	Averaged maximum rainfall intensity (mm/h)
< 100 m	989.2	27.6	163.2	0.82
100 – 500 m	1483.1	53.1	156.0	1.01
500 – 1500 m	2821.4	83.3	545.3	5.58
1500 – 2500 m	3101.5	81.3	869.2	9.82
> 2500 m	2226.5	32.3	741.7	7.54

Table 2 Model simulated 72-h averaged maximum and averaged rainfall and rain intensity at different altitudes.

Figure 9 shows the model simulated 72-hour averaged rainfall rate and accumulated rainfall over land and over ocean for the control case, warm-rain only, improved microphysics, YSU-PBL, no-PBL cases. The results indicated that averaged rain rate is quite weak after 48-hour model integration over the ocean for all cases. Both averaged rainfall and rainfall intensity are larger over land than those over ocean. Again these results suggest that the terrain-induced circulation favors stronger precipitation processes and rainfall. The rainfall intensity and rainfall simulated by the warm ran only, improved microphysics and YSU-PBL are larger than the control run over land. YSU-PBL case also simulated larger and stronger rain intensity and rainfall over ocean. Two No-PBL cases (one tune off PBL in all three domains, and the other turn off the PBL in the 2-km grid domain) simulated much less rain over the land compared to cases with PBL.

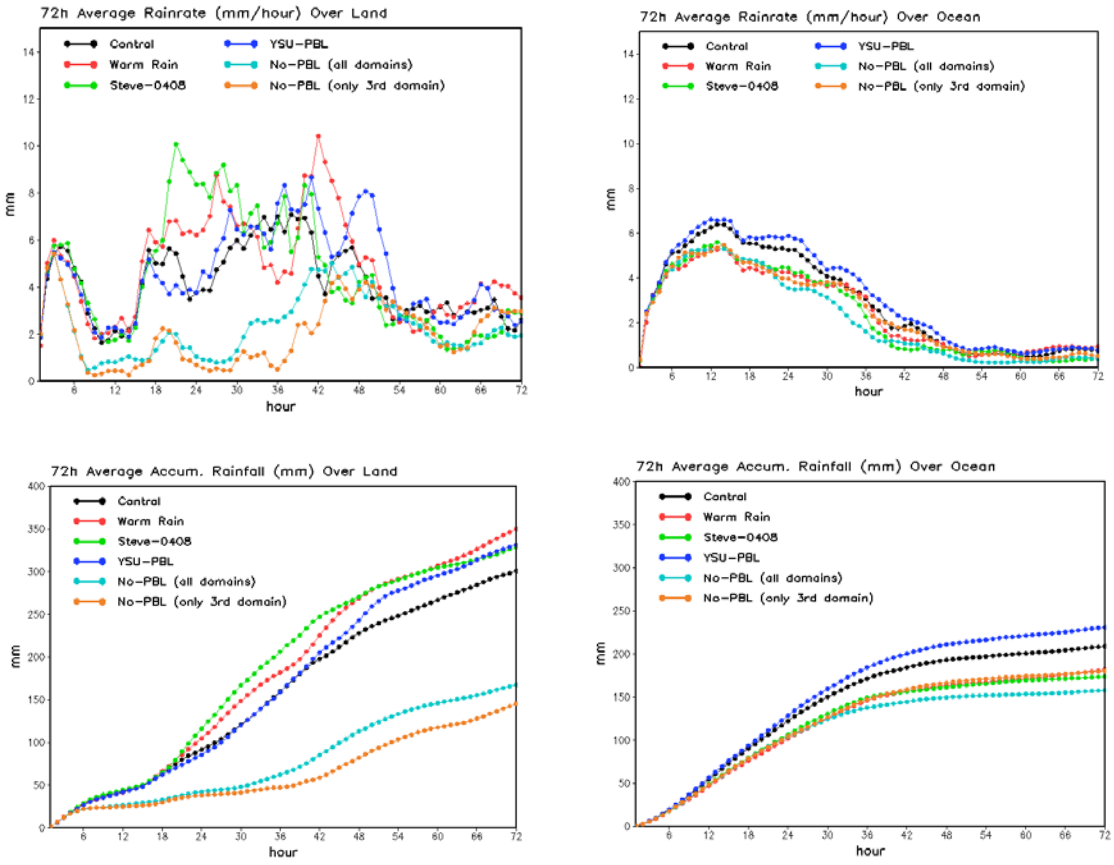

Fig. 9 Model simulated 72-hour averaged rainfall rate over land (upper-left panel) and over ocean (upper-right panel) associated with different cases. The lower panels are the same as upper panels except for the averaged accumulated rainfall.

We have conducted several sensitivity tests on the impact of microphysics schemes, terrain heights and sea surface temperature on the heavy rainfall (especially over South Taiwan) associated with Typhoon Morakot. The major highlights are as follows (see Table 3):

1. Microphysical processes cannot determine the location of heavy precipitation, but it can affect the intensity and total amount of rainfall.

2. Improved microphysics (reduced 40 dBZ aloft and amount graupel) could reduce (increase) the amount of precipitation over the plain and low terrain region (high terrain and east side) of S. Taiwan.

3. The ice processes are not important for heavy precipitation over S. Taiwan.

4. Sea surface temperatures (SSTs) cannot determine the location of heavy precipitation, but they too can affect the total amount of rainfall. SSTs on the southwest side of Taiwan have more impact on the rainfall over southern Taiwan than those east of the island (Fig. 10).

5. A 2 degree increase (decrease) in SST can increase (decrease) rainfall over southern Taiwan by 16-20% (6-16%).

6. Terrain height can also affect the amount of rainfall over southern Taiwan. Reducing the terrain height by 25, 50 (see Fig. 10), and 75% reduces the amount of heavy rainfall by 16, 27 and 39%, respectively. Topographic areas seem to be affected more by reductions in the terrain height. Both (eastern and western) coastal regions generally have more rainfall when the terrain height is reduced.

7. The typhoon-induced circulation and Taiwan's unique terrain determined the location of heavy precipitation

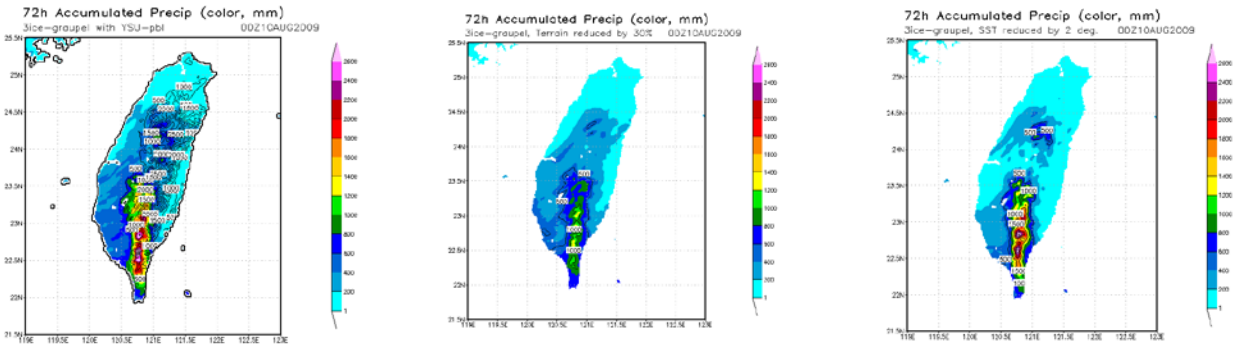

Fig. 10 Model simulated accumulated rainfall from August 6 0000UTC to August 9 0000UTC 2009. The YSU –PBL case (left), 50% reduced terrain height case (middle) and 2^{o} SST – South China Sea case (right) are shown.

	48 – hours Maximum Rainfall (mm)	72-hours Maximum Rainfall
3ICE-Graupel	**2856**	**3345**
YSU PBL	**2125**	**3201**
Reduced SST by 2^o – Southwest of Taiwan	**2657**	**3129**
Reduced SST by 2^o – West of Taiwan	**2720**	**3225**
Reduced SST by 2^o – East of Taiwan	**2451**	**2895**
Increased SST by 2^o – Southwest of Taiwan	**2457**	**3321**
Increased SST by 2^o – West of Taiwan	**2488**	**3395**
Increased SST by 2^o – East of Taiwan	**2827**	**3274**
Reduced Terrain height by 25%	**1948**	**2163**
Reduced Terrain height by 50%	**1209**	**1332**
Reduced Terrain height by 75%	**917**	**973**
Reduced Terrain height by 99%	**802**	**809**
Observation	**2143**	**2434**

Table 3 The maximum rainfall simulated by model with different Goddard microphysical options (include improved as described in Section 2.1). Observed maximum rainfall is also shown for comparison.

Note that we are in the process to write two parts of paper associated with Typhoon Morakot case. These papers will be submitted to a special journal for Morakot case to be published by the *Terrestrial, Atmospheric and Oceanic Sciences (TAO).*

3.2 Conduct case study (Terrain-influenced Monsoon Rainfall Experiment, TiMREX)

Several major precipitation events (i.e., observed during the SoWMEX/TiMREX 2008) that developed over the Taiwan region were selected for examining the performance of the cloud microphysics parameterization on precipitation processes and its predicted rainfall. The selection of these cases will be consulted with CWB operational forecasters and researchers. For example, Co-PI., Ms. Chang, has conducted case study (IOP8 and see Table 4) observed during SoWMEX/TiMREX in 2008. Sensitivity tests are performed to examine the impact of cumulus parameterization and PBL scheme on simulated rainfall amount and patterns (Table 5). The WRF V3.1 with improved microphysics is used to simulate this typhoon case. Figure 11 shows the WRF domain, with 45, 15 and 5 km, respectively. The surface heat and moisture fluxes (from both ocean and land) were computed from similarity theory (Monin and Obukhov 1954). The land surface model is based on Noah LSM. The Goddard broadband two-stream (upward and downward fluxes) approach was used for the shortwave radiative flux calculations (Chou and Suarez 1999). The model was initialized from NOAA/NCEP/GFS global analyses (1.0^o by 1.0^o). Time-varying lateral boundary conditions were provided at 6-h intervals.

IOP#	Date	Science objectives
1 (a & b)	06Z May 19 to 00Z May 22	Frontal circulation Upstream environment for orographic convection Model verification and data assimilation
2	06Z May 27 to 21Z May 29	Southwest flow interacting with the terrain Upstream condition for mountain convection Lee side vortex/shear zone
3	21Z May 29 to 12Z May 31	Island effects on SW (LLJ) and the Mei-Yu front Upstream condition forheavy precipitation
4	21Z June 1 to15Z June 3	Mesoscale convective systems Shallow surface front Mesoscale convective vortex
5	18Z June 3 to 12Z June 4	Mesoscale convective systems Quasi-stationary front Mesoscale convective vortex
6	18Z June 4 to 12Z June 6	Mesoscale convective systems Quasi-stationary front Mesoscale convective vortex
7	00Z June 12 to 12Z June 13	Convection initiation Orographic convection
8	**00Z June 14 to 12Z June 17**	**Southwesterly flow interacting with the terrain** **Upstream condition for mountain convection, low level jet** **Mesoscale convective systems** **Mesoscale convective vortex**
9	06Z June 23 to 12Z 26 June	Typhoon Fengseng track uncertainty Typhoon induced southwesterly flow and related heavy rain systems

Table 4 The summary of SoWMEX/TiMREX IOP cases (kindly provided by Dr. Pay-Liam Lin). Red indicated the case (IOP8) has been conducted by Ms. Mei-Yu Chang.

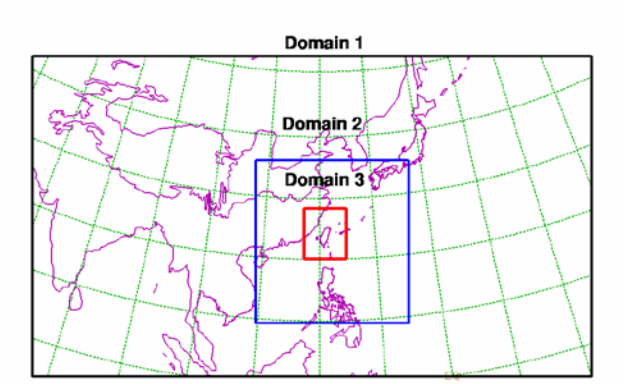

Fig. 11 WRF Inter-nesting model configuration used for SoWMEX case. Horizontal resolutions for domains are 45, 15 and 5 km, respectively.

Case	PBL Scheme	Cumulus Scheme
YK	YSU	Kain and Fritsch (KF)
YB	YSU	Betts-Miller-Janjic (BMJ)
YG	YSU	Grell and Devenyi (GD)
MK	MYJ	Kain and Fritsch
MB	MYJ	Betts-Miller-Janjic
MG	MYJ	Grell and Devenyi

Table 5 The sensitivity tests of the PBL and cumulus parameterization schemes for SoWMEX case.

Figure 12 shows the observed and model simulated rainfall amount and pattern. The simulated heavy rainfall from YG (YSU PBL and Grell and Devenyi cumulus scheme), YK (YSU PBL

and Kain and Fritsch cumulus scheme), MG (BMJ PBL and Grell and Devenyi cumulus scheme) and MK (MYJ PBL and Kain and Fritsch cumulus scheme) is mainly over the southern region of Taiwan as seen in observation. In addition, all experiments also simulated secondary heavy rainfall over the northern Taiwan. However, there are notable differences between these simulations in terms of the rainfall amount and pattern. The case using the MYJ PBL and Kain and Fritsch cumulus scheme has better performance in rainfall forecast. On the other hand, the two cases with Beets-Miller-Janjic parameterization scheme (YB and MB) has a maximum rainfall occurred in the central Taiwan region. The BMJ scheme is known for better simulation over North America. This is because the temperature and humidity are tuned for typical sounding over North America.

PI and Co-PI[4] plan to continue conducting detailed analyses and comparisons with observations (SoWMEX/TiMREX cases). We will evaluate model forecasts with ground-based observations (i.e., radar, rain gauge) and satellite data. Model estimates of radar reflectivity will be produced from the simulated precipitation using the characteristics of the microphysics properties (i.e., hydrometeor type, size distribution). Actual radar reflectivity (in convective or heavy rainfall region and stratiform or light rainfall region) can then be interpolated to WRF grid to facilitate comparisons similar to the QPF evaluations. We will use the contoured frequency with altitude diagrams (CFADs)[5] to examine the frequency distributions of various fields as a function of height. The validation of model microphysics needs to work with CWB operational group.

In addition, sensitivity tests will be conducted to examine the impact of the model resolution, microphysics, PBL and convective parameterization on rainfall and patterns associated with heavy rainfall events (i.e., one more case from SoWMEX/TiMREX 2008).

[4] The co-I will focus on the PBL and microphysics processes for her Ph. D. thesis.

[5] This CFAD program including the subroutine for computing radar reflectivity has been provided to Co-PI. Ms. Mei-Yu Chang.

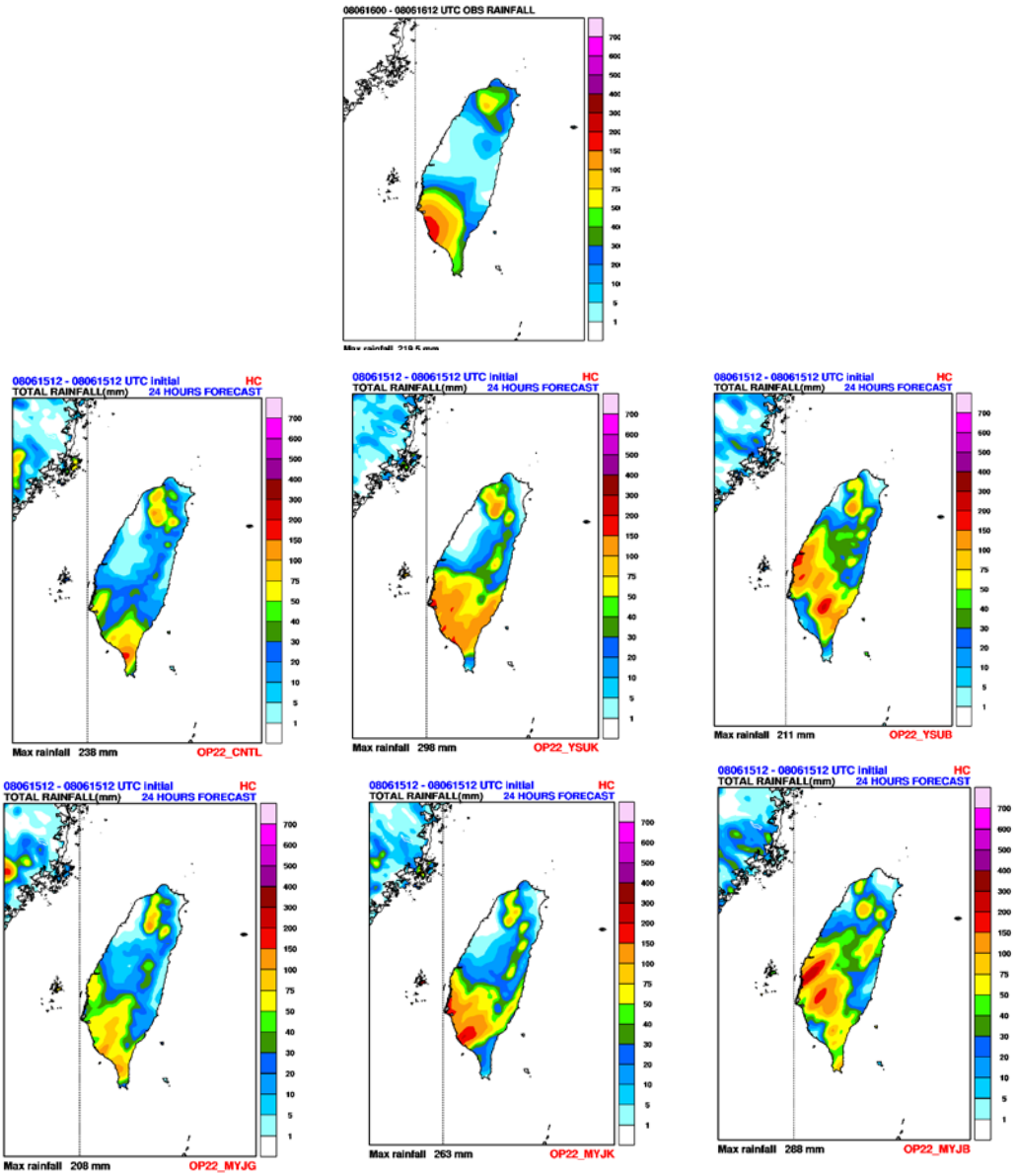

Fig. 12 CWB's WRF simulated surface rainfall (mm) WRF simulated accumulated surface rainfall (mm) between 12 Z (UTC) June 15 to 12 Z June 18 2008 using Goddard 3ICE microphysical scheme. Top panel shows the observed rainfall. Middle panels are YK (left), YB (middle) and YG-control (right). Bottom panels are MK (left), MK (middle) and MB (right).

4. CWB Visit

The PI, W.-K. Tao, has visited the CWB and worked with Ms. Chang the week of February 22 2010. He also presented a talk to CWB and its title is "*The impact of microphysics on precipitation associated with Typhoon Morakot 2009*". In this talk, he presented: (a) the results from very high-resolution WRF simulation for Typhoon Morakot case, (b) The impact of microphysics schemes on rainfall intensity and patterns on a heavy precipitation event in Taiwan, and (c) The high temporal (72 s) and special (2 km) visualization of cloud species, radar reflectivity, surface fluxes and tracer for Morakpt case.

During the visit to CWB, Tao has provided the new improvement of microphysical processes to the Co-I. Ms. Mei-Yu Chang of CWB. Ms. Chang has implemented these improvements into CWB's WRF (V3.1). Tao also discussed the PBL and cumulus parameterization with Co-I.. In June, Dr. Tao visited Ms. Chang to discuss the proposed research in terms of cases, and sensitivity tests needed to be conducted.

5. Reference (not complete, will provide as requested)

Ackerman, T. P., K.-N. Liou, F. P. J. Valero and L. Pfister, 1988: Heating rates in tropical anvils. *J. Atmos. Sci.*, **45**, 1606-1623.

Arakawa, A. and W. H. Schubert, 1974: Interaction of cumulus cloud ensemble with the large-scale environment. Part I. *J. Atoms. Sci.*, **31**, 674-701.

Betts, A. K., 1986: A new convective adjustment scheme. Part I: Observational and theoretical basis. Quart. J. Roy. Meteor. Soc., 112, 677–691.

Betts, A. K., andM. J. Miller, 1986: A new convective adjustment scheme. Part II: Single column tests using GATE wave, BOMEX, and arctic air-mass data sets. Quart. J. Roy. Meteor. Soc., 112, 693–709.

Chou, M.-D., and M. J. Suzrez (2001): A thermal infrared radiation parameterization for atmospheric studies. NASA/TM-2001-10406, vol. 19, 55 pp

Chou, M.-D., and L. Kouvaris, 1991: Calculations of transmission functions in the IR CO2 and O3 Bands. *J. Geophys. Res.*, **96**, 9003-9012.

Chou, M.-D., W. Ridgway, and M.-H. Yan, 1995: Parameterizations for water vapor IR radiative transfer in both the middle and lower atmospheres. *J. Atmos. Sci.*, **52**, 1159-1167.

Chou, M.-D., and M. J. Suarez, 1999: A shortwave radiation Parameterization for atmospheric studies. 15, NASA/TM-104606. pp40.

Chou, M.-D., K.-T. Lee, S.-C. Tsay, and Q. Fu, 1999: Parameterization for cloud longwave scattering for use in atmospheric models. *J. Climate*, **12**, 159-169.

Chou, M.-D., and M. J. Suzrez (1999): A solar radiation parameterization for atmospheric studies. NASA Tech. Pre. NASA/TM-1999-10460, vol. 15, 38 pp

Cotton, W. R., M. A. Stephens, T. Nehrkorn and G. J. Tripoli, 1982: The Colorado State University three-dimensional cloud-mesoscale model-1982. Part II: An ice-phase parameterization. *J. Rech. Atmos.*, **16**, 295-320.

Cotton, W. R., G. J. Tripoli, R. Rauber and E. Mulvihill, 1986: Numerical simulation of the effects of varying ice crystal nucleation rates and aggregation processes on orographic snowfall. *J. Climate Appl. Meteor*., **25**, 1658-1680.

Ferrier, B. S., 1994: A double-moment multiple-phase four-class bulk ice scheme. Part I: Description. *J. Atmos Sc.i*, **51**, 249-280.

Ferrier, B.S., W.-K. Tao and J. Simpson,1995: A double-moment multiple-phase four-class bulk ice scheme. Part II: Simulations of convective storms in different large-scale environments and comparisons with other bulk parameterizations. *J. Atmos Sci.*, **52**, 1001-1033.

Fritsch, J. M., and C. F. Chappell, 1980: Numerical prediction of convectively driven mesoscale pressure systems. Part I: Convective parameterization. *J. Atmos. Sci.*, **37**, 1722-1733.

Fritsch, J. M., and R. E. Carbone, 2002: Research and development to improve quantitative precipitation forecasts in the warm season: A synopsis of the March 2002 USWRP

Workshop and statement of priority recommendations. *Technical report to UEWRP Science Committee,*134pp.

Gallus, W. A., Jr., 1999: Eta simulations of three extreme precipitation events: Sensitivity to resolution and convective parameterization. *Wea. Forecasting,* **14**, 405-426.

Grell, G. A., and D. Devenyi, 2002: A generalized approach to parameterizing convection combining ensemble and data assimilation techniques. Geophys. Res. Lett., 29(14), Article 1693.

Hong S.-Y., and H.-L. Pan, 1996: Nonlocal boundary layer vertical diffusion in a medium-range forecast model. *Mon. Wea. Rev.*, **124**, 2322–2339.

Hong, S.Y., Y. Noh, and J. Dudhia (2006), A New Vertical Diffusion Package with an Explicit Treatment of Entrainment Processes, *Mon. Wea. Rev.*, 134, 2318–2341.

Janjic, Z. I., 1990: The step-mountain coordinate: physical package, Mon. Wea. Rev., 118, 1429–1443.

Janjic, Z. I., 1994: The step-mountain eta coordinate model: further developments of the convection, viscous sublayer and turbulence closure schemes, Mon. Wea. Rev., 122, 927–945.

Janjic, Z. I., 1996: The surface layer in the NCEP Eta Model, Eleventh Conference on Numerical Weather Prediction, Norfolk, VA, 19–23 August; Amer. Meteor. Soc., Boston, MA, 354–355.

Janjic, Z. I., 2000: Comments on "Development and Evaluation of a Convection Scheme for Use in Climate Models", J. Atmos. Sci., 57, p. 3686.

Janjic Z. I., 2002: Nonsigular implementation of the Mellor-Yamada level 2.5 scheme in the NCEP global model. NCEP Office Note 437, 61 pp. [Available at NCEP/EMC, 5200 Auth Road, Camp Springs, MD 20746.].

Kain, J. S., and J. M. Fritsch, 1990: A one-dimensional entraining/ detraining plume modeland its application in convective parameterization, J. Atmos. Sci., 47, 2784–2802.

Kain, J. S., and J. M. Fritsch, 1993: Convective parameterization for mesoscale models: The Kain-Fritcsh scheme, The representation of cumulus convection in numerical models, K. A. Emanuel and D.J. Raymond, Eds., Amer. Meteor. Soc., 246 pp

Koenig, L. R., and F. W. Murray 1976: Ice-bearing cumulus cloud evolution: Numerical simulation and general comparison against observations. *J. Appl. Meteor*., **15**, 747-762.

Kratz, D. P., M.-D. Chou, M. M.-H. Yan, and C.-H. Ho, 1998: Minor trace gas radiative forcing calculations using the k-distribution method with one-parameter scaling. *J. Geophy. Res.*, **103**, 31647-31656.

Lang, S., **W.-K. Tao**, R. Cifelli, W. Olson, J. Halverson, S. Rutledge, and J. Simpson, 2007: Improving simulations of convective system from TRMM LBA: Easterly and Westerly regimes. *J. Atmos. Sci.,* **64**, 1141-1164.

Li, X., W.-K. Tao, A. Khain, J. Simpson and D. Johnson, 2009: Sensitivity of a cloud-resolving model to bulk and explicit-bin microphysics schemes: Part I: Comparisons. *J. Atmos. Sci*., **66**, 3-21**.**

Li, X., W.-K. Tao, A. Khain, J. Simpson and D. Johnson, 2009: Sensitivity of a cloud-resolving model to bulk and explicit-bin microphysics schemes:: Part II: Cloud microphysics and storm dynamics interactions. *J. Atmos. Sci*., **66**, 22-40.

Lin, Y.-L., R. D. Farley and H. D. Orville, 1983: Bulk parameterization of the snow field in a cloud model. *J. Clim. Appl. Meteor.*, **22**, 1065-1092.

Liu, Y., D.-L. Zhang, and M. K. Yau, 1997: A multiscale numerical study of Hurricane Andrew (1992)/ Part I: An explicit simulation. *Mon. Wea. Rev.*, **125**, 3073-3093.

McCumber, M., W.-K. Tao, J. Simpson, R. Penc, and S.-T. Soong, 1991: Comparison of ice-phase microphysical parameterization schemes using numerical simulations of tropical convection. *J. Appl. Meteor*., **30**, 985-1004.

Mellor, G. L., and T. Yamada, 1982: Development of a turbulence closure model for geophysical fluid problems. Rev. Geophys. Space Phys., 20, 851–875.

Molinari, J., and M. Dudek, 1992: Parameterization of convective precipitation in mesoscale numerical models: A critical review. *Mon. Wea. Rev.*, **120**, 326-344.

Noh, Y., W. G. Cheon, S.-Y. Hong, and S. Raasch (2003), Improvement of the K-profile model for the planetary boundary layer based on large eddy simulation data, *Bound.-Layer Meteor., 107*, 401–427.

Orville, H. D., and F. K. Kopp 1977: Numerical simulation of the life history of a hailstorm. *J. Atmos. Sci*., **34**, 1596-1618.

Rogers, R. F., and J. M. Fritsch, 1996: A general framework for convective trigger function. *Mon. Wea. Rev*., **124**, 2438-2452.

Rutledge, S.A., and P.V. Hobbs, 1983: The mesoscale and microscale structure and organization of clouds and precipitation in mid-latitude clouds. Part VIII: A model for the "seeder-feeder" process in warm-frontal rainbands. *J. Atmos. Sci*., **40**, 1185-1206.

Rutledge, S.A., and P.V. Hobbs, 1984: The mesoscale and microscale structure and organization of clouds and precipitation in mid-latitude clouds. Part XII: A diagnostic modeling study of precipitation development in narrow cold frontal rainbands. *J. Atmos. Sci.*, **41**, 2949-2972.

Smagorinsky, J. (1963), General circulation experiments with the primitive equations, *Mon. Wea. Rev., 91*, 99–164.

Stephens, G. L., 1978, Radiative profiles in extended water clouds. Part II: Parameterization schemes. *J. Atmos. Sci.*, **35**, 2123-2132.

Stephens, G. L., 1984: The parameterization of radiation for numerical weather prediction and climate models. *Mon. Wea. Rev*., **112**, 826-867.

Tao, W.-K., and S.-T. Soong, 1986: A study of the response of deep tropical clouds to mesoscale processes: Three-dimensional numerical experiments. *J. Atmos. Sci.*, **43**, 2653-2676.

Tao, W.-K., J. Simpson, and S.-T. Soong, 1987: Statistical properties of a cloud ensemble: A numerical study. *J. Atmos. Sci.*, **44**, 3175-3187.

Tao, W.-K., and J. Simpson, 1989: Modeling study of a tropical squall-type convective line. *J. Atmos. Sci.*, **46**, 177-202.

Tao, W.-K., and J. Simpson, 1993: The Goddard Cumulus Ensemble Model. Part I: Model description. *Terrestrial, Atmospheric and Oceanic Sciences,* **4**, 19-54.

Tao, W.-K., J. Scala, B. Ferrier and J. Simpson, 1995: The effects of melting processes on the development of a tropical and a midlatitude squall line, *J. Atmos. Sci.,* **52**, 1934-1948.

Tao, W.-K., 2003: Goddard Cumulus Ensemble (GCE) model: Application for understanding precipitation processes, *AMS Meteorological Monographs - Cloud Systems, Hurricanes and TRMM*, 107-138.

Tao, W.-K., J. Simpson, D. Baker, S. Braun, M.-D. Chou, B. Ferrier, D. Johnson, A. Khain, S. Lang, B. Lynn, C.-L. Shie, D. Starr, C.-H. Sui, Y. Wang and P. Wetzel, 2003a: Microphysics, Radiation and Surface Processes in a Non-hydrostatic Model, *Meteorology and Atmospheric Physics,* **82**, 97-137.

Tao, W.-K., D. Starr, A. Hou, P. Newman, and Y. Sud, 2003b: Summary of cumulus parameterization workshop, *Bull. Amer. Meteor. Soc.,* **84**, 1055-1062.

Tao, W.-K., C.-L. Shie, D. Johnson, R. Johnson, S. Braun, J. Simpson, and P. E. Ciesielski, 2003c*:* Convective Systems over South China Sea: Cloud-Resolving Model Simulations *J. Atmos. Sci.*, **60**, 2929-2956.

Wang, W., and N. L. Seaman, 1997: A comparison study of convective parameterization schemes in a mesoscale model. *Mon. Wea. Rev*., **125**, 252-278.

Weisman, M. L., W. C. Skamarock and J. B. Klemp, 1997: The resolution dependence of explicitly modeled convective systems. *Mon. Wea. Rev*., **125**, 527-548.

Xu, K.-M., and A. Arakawa, 1992: Semiprognostic tests of Arakawa-Schubert cumulus parameterization using simulated data. *J. Atmos. Sci.*, **49**, 2421-2436.

Yang, M.-J., and Q.-C. Tung, 2003: Evaluation of rainfall forecasts over Taiwan by four cumulus parameterization schemes. *J. Meteor. Soc. Japan*, **81**, 1163-1183.

Yuter, S. and R. A. Houze Jr., 1995: Measurements of Raindrop Size Distributions over the Pacific Warm Pool and Implications for Z-R Relations, *J. Appl. Meteor*., 36, 847-867.

Zhang, D.-L., and X. Wang, 2004: Dependence of hurricane intensity and structures on vertical resolution and time step size. *Adv. Atmos. Sci*., 5, 711-725.